AIP Journal of Applied Physics

A monoclinic-tetragonal ferroelectric phase transition in lead-free (K0.5Na0.5)NbO3-x%LiNbO3 solid solution

Wenwei Ge, Yang Ren, Jialiang Zhang, Christopher P. Devreugd, Jiefang Li, and D. Viehland

Citation: Journal of Applied Physics **111**, 103503 (2012); doi: 10.1063/1.4716027
View online: http://dx.doi.org/10.1063/1.4716027
View Table of Contents: http://scitation.aip.org/content/aip/journal/jap/111/10?ver=pdfcov
Published by the AIP Publishing

A monoclinic-tetragonal ferroelectric phase transition in lead-free $(K_{0.5}Na_{0.5})NbO_3$-x%$LiNbO_3$ solid solution

Wenwei Ge,[1,a)] Yang Ren,[2] Jialiang Zhang,[3] Christopher P. Devreugd,[1] Jiefang Li,[1] and D. Viehland[1]
[1]*Department of Materials Science and Engineering, Virginia Tech, Blacksburg, Virginia 24061, USA*
[2]*Advanced Photon Source, Argonne National Laboratory, Argonne, Illinois 60439, USA*
[3]*School of Physics, State Key Laboratory of Crystal Materials, Shandong University, Jinan 250100, People's Republic of China*

(Received 14 August 2011; accepted 14 April 2012; published online 16 May 2012)

A monoclinic ferroelectric phase with space group *Pm* has been discovered in lead-free $(K_{0.5}Na_{0.5})NbO_3$-5%$LiNbO_3$ solid solution ceramics by high energy synchrotron x-ray powder diffraction measurements. At ambient temperature, the lattice parameters of this monoclinic structure were $(a_m, b_m, c_m; \beta) = (4.015\ Å, 3.944\ Å, 3.987\ Å; 90.34^\circ)$. This monoclinic phase transformed to a tetragonal (*P4mm*) one on heating between 340 K and 360 K. The results demonstrate the presence of structurally bridging low symmetry monoclinic phase in $(K_{0.5}Na_{0.5})NbO_3$-x%$LiNbO_3$ solid solution system: indicating a means to achieve high piezoelectricity in Pb-free systems via domain engineering. © *2012 American Institute of Physics*. [http://dx.doi.org/10.1063/1.4716027]

I. INTRODUCTION

Ceramics based on $(K,Na)NbO_3$ have attracted considerable attention as an important type of lead-free piezoelectric material in recent years because of their excellent piezoelectric properties.[1–12] In particular, some (K,Na,Li)(Nb,Ta,Sb)O_3 ceramics exhibit longitudinal piezoelectric coefficients of $d_{33} \geq 400$ pC/N,[1,13] which is nearly comparable with that of "soft" $Pb(Zr,Ti)O_3$ materials such as PZT-5A.[14–16]

The phase diagram for solid solutions of $K_xNa_{1-x}NbO_3$ has been extensively studied.[17–24] The sequence of phase transitions of the $KNbO_3$ end-member on cooling is cubic (C, $Pm\bar{3}m$) $\overset{\sim 420\,^\circ C}{\longrightarrow}$ tetragonal (T, *P4mm*) $\overset{\sim 220\,^\circ C}{\longrightarrow}$ orthorhombic (O, *Amm*2) $\overset{\sim 10\,^\circ C}{\longrightarrow}$ rhombohedral (R, *R*3*m*).[17,19,23] The phase stability of the $NaNbO_3$ end-member had also been shown to be quite complicated.[25,26] $NaNbO_3$ is antiferroelectric phase with an O structure (Pbma) at room temperature. It transforms to a high-temperature paraelectric phase with an O structure (Pmnm) at T_c=365 °C, and to a low-temperature ferroelectric phase with a R structure (R3c) at −100 °C. Between 365 °C and 575 °C, $NaNbO_3$ undergoes three O phases transformations, transforms to a T structure (P4bm) near 575 °C, and finally to a C structure ($Pm\bar{3}m$) near 640 °C. However, the phase diagram of $K_xNa_{1-x}NbO_3$ resembles that of $NaNbO_3$ only over a small composition range for $x < 0.02$.[19] For $x \geq 0.02$, the initial structure is changed, based on $NaNbO_3$, towards one based on $KNbO_3$. In the phase diagram, three separate phase boundaries at room temperature have been identified at $x = 0.175$, 0.325, and 0.475 by using thermal analysis and x-ray diffraction.[18,19] The phase boundary at $x = 0.475$ separates two O phases: the best piezoelectric properties are found for compositions close to this phase boundary near $x = 0.5$.[27] Accordingly, most of the recent investigations of $K_xNa_{1-x}NbO_3$ based ceramics have been carried out based on this nearly equal molar ratio of K:Na = 1:1.[28–35] Single crystal x-ray diffractions have shown that $K_{0.5}Na_{0.5}NbO_3$ (KNN) undergoes a similar phase transformation sequence as $KNbO_3$,[31] where an O (*Amm*2) structure is stable at room temperature with lattice parameters of (a, b, c) = (5.6395, 3.9399, 5.6725) Å.[17,18,36] The pseudo-cubic perovskite unit cell for KNN could be considered as a special case of a monoclinic structure (i.e., pseudo-monoclinic) with lattice parameters $a_m = c_m > b_m$, where b_m is perpendicular to the a_m and c_m planes and the monoclinic angle β is slightly more than 90°: $a_m = c_m = 4.000$ Å, $b_m = 3.940$ Å, and $\beta = 90.34^\circ$.[16,17,36,37] Baker *et al.*[23] found, using x-ray diffraction, that the room temperature structure of $0.2 \leq x \leq 0.4$ could be refined with a monoclinic (M, Pm) symmetry having $a^0b^+c^0$ tiltings of the oxygen octahedra, following the Glazer notation.[38] For $x > 0.4$, the octahedral tilts disappeared. The full width at half maximum (FWHM) of the pseudocubic (200)/(002) peaks decreased gradually with increasing x between 0.45 and 0.55 and reached the minimum value and remained constant for $x \geq 0.55$.[23] Thus, it is proposed that $K_xNa_{1-x}NbO_3$ has a M structure for $0.4 < x < 0.55$, as the pseudocubic (200)/(002) peaks should completely overlap ($a_m = c_m$) for an O (*Amm*2) structure. These results are consistent with a structure refinement with M (Pm) symmetry for $0.4 \leq x \leq 0.6$, as previously reported by Tellier *et al.*[24] However, the differences between the M (Pm) and O (Amm2) structures are quite small in both cases.[23,24] Thus, many publications report the use of an O structure for the refinements of the cell parameters of KNN-based materials at room temperature.

Pure KNN ceramics prepared by conventional solid-state reaction method show relatively lower electrical properties ($d_{33} \sim 80$ pC/N, kp ~ 36%) due to the difficulty in the processing of dense ceramics.[39] Thus, a variety of substituents (including $LiNbO_3$, $LiTaO_3$ and $LiSbO_3$) have been added to KNN to form new KNN-based ceramics with improved relative densities and piezoelectric properties.[6,9,10,12,40–42] Due to

a)Electronic mail: wenweige@vt.edu.

the expensive price of Ta_2O_5 and toxicity of Sb element, $LiNbO_3$ has been regarded as the most promising substituent amongst these possibilities.[41] In the $(K_{0.5}Na_{0.5})NbO_3$-x%$LiNbO_3$ (or KNN-x%LN) solid solution, the highest d_{33} values have been reported in the composition range of $5 \leq x \leq 7$.[1–3,39–41,43–45] Structural investigations by conventional x-ray powder diffraction (XRPD) measurements at ambient temperatures revealed that KNN-x%LN has an orthorhombic (O) structure for $x < 5$ that transforms to tetragonal (T) with increasing LN content at $x > 7$.[2,42] For $5 \leq x \leq 7$, a coexistence of O and T phases has been reported.[2,4] Temperature dependent piezoelectric measurements have shown maximum piezoelectric properties near a narrow temperature range about this polymorphic T→O boundary. Enhancements in d_{33} by compositional modifications have been shown to result from a shifting of the T→O phase boundary to lower temperatures: from ~210 °C for pure KNN, to near room temperature for those with the highest d_{33} values.[4,46,47]

Monoclinic (M) phases are well known in Pb-based perovskites that are sandwiched between ferroelectric R and T phases near a morphotropic phase boundary (MPB).[48–51] These M phases are believed to be important to the high piezoelectricity of MPB systems, as the lower symmetry allows the polarization to rotate between pseudocubic ⟨111⟩ and ⟨001⟩ directions.[52–54] Various types of monoclinic structures have been reported in Pb-based systems, [48,51,54,55] including M_A, M_B, and M_C: which belong to the space groups *Cm*, *Cm*, and *Pm*, respectively. The M_A, M_B, and M_C notations are adopted following Vanderbilt and Cohen.[56] The M_A and M_B unit cells have a unique *bm* axis along the ⟨110⟩ direction and are doubled and rotated 45° about the *c*-axis, with respect to the pseudocubic cell;[56] whereas the M_C unit cell is primitive having a unique *bm* axis that is oriented along the pseudocubic ⟨010⟩.[56] Although both the M_A and M_B phases belong to the *Cm* space group, the difference lies in the magnitudes of the components of the polarization corresponding to the pseudocubic cell: for the M_A phase, $Px = Py < Pz$, whereas for the M_B phase, $Px = Py > Pz$.[56]

The excellent piezoelectric properties of ⟨001⟩ grain-oriented KNN-based ceramics[1,5] for compositions close to the PPB may be the result of "domain-engineered" states, whose structural origins are as yet unidentified. In order to elucidate the mechanism for high piezo-responses in the KNN-based non-Pb systems, it is important to develop a structural understanding of induced phase transitions in the PPB region. Structural studies by conventional XRPD of KNN-x%LN ceramics for $5 \leq x \leq 7$ have indicated the coexistence of T and O phases.[2,4,37] Recently, Klein *et al.*[35] reported that the crystal structure of KNN-x%LN is similar to KNN for $x < 5$, where a M phase appears for $5 \leq x \leq 10$ as determined by Raman spectroscopy. But structural investigations by high energy synchrotron x-rays have yet to be reported: such studies would be more powerful with regards to high precision structural determination near phase boundaries, as previously demonstrated for PZT.[48] Considering that proper understanding of the correlation between structure and properties is crucial in developing new materials, here, we have performed synchrotron x-ray powder diffraction measurements for KNN-5%LN ceramics and found that the room temperature structure of KNN-5%LN is in fact monoclinic belonging to the space group *Pm* and with lattice parameters of $a_m = 4.015$ Å, $b_m = 3.944$ Å, $c_m = 3.987$ Å, and $\beta = 90.34°$.

II. EXPERIMENTAL PROCEDURE

Ceramics of KNN-5%LN were prepared by a conventional solid-state reaction method using high purity (≥99.9%) K_2CO_3, Na_2CO_3, Li_2CO_3, and Nb_2O_5 starting reagents. All the starting reagents were dried in a vacuum oven at 120 °C for 8 h and subsequently weighed according to the formulation. The powders were ball milled in anhydrous ethanol for 12 h, and then calcined at 850 °C for 5 h. The calcined powders were again ball milled for 12 h and pressed into pellet disks of 15 mm in diameter and 1.5 mm in thickness at 160 MPa. Finally, these pellets were sintered in air at 1050°~1100 °C for 2 h and furnace cooled. During sintering, to avoid possible alkali evaporation, the pellets were buried in powders of the same chemical compositions and were covered by a reversed-crucible that was further sealed by the ZrO_2 power. The surface microstructures of sintered ceramics were characterized on a LEO (Zeiss) 1550 scanning electronic microscope (SEM). Sintered ceramic samples were ground to yield parallel plates of 0.6 mm thickness and polished with 0.3 μm diamond paste to a smooth surface finish. To eliminate residual stress induced by the grinding and polishing, the samples were annealed in air at 550 °C for 1 h and then slowly cooled to room temperature. Silver electrodes were deposited on both surfaces and air-dried. Temperature-dependent dielectric constant measurements were then performed using a multiple-frequency LCR meter (HP 4284A).

In addition, x-ray diffraction studies were performed on ceramic plates with a 0.6 mm thickness on beam line 11-ID-C ($\lambda = 0.10798$ Å and E = 114.8 keV) at the advanced photon sources (Argonne National Laboratory). Due to the large penetration depth of high-energy x-rays, diffraction information is collected from the bulk of the samples. The beam size was set to be 0.3×0.3 mm^2 by tungsten slits. The diffraction images were collected in the forward direction using a Perkin-Elmer large area detector. Temperature dependent measurements were performed in the temperature range of 280 to 420 K by mounting the samples on a glass pedestal and loading them into a closed-cycle N_2 cryostat, which had an estimated temperature accuracy of 2 K and stability better than 0.1 K. Two-dimensional diffraction images were integrated using the software package FIT2D, in order to obtain one-dimensional diffraction patterns of two-theta scan.[57] Crystal structure analysis was carried out by Rietveld refinement using the GSAS program package.[58] Pseudo-Voigt peak shape[59] and cosine Fourier series background functions were chosen. The wavelength and instrumental parameters were determined by refining the profiles from standard CeO_2 samples.

III. RESULTS AND DISCUSSION

Figure 1 shows the SEM images of KNN-5%LN ceramics. The KNN-5%LN ceramics show well faceted

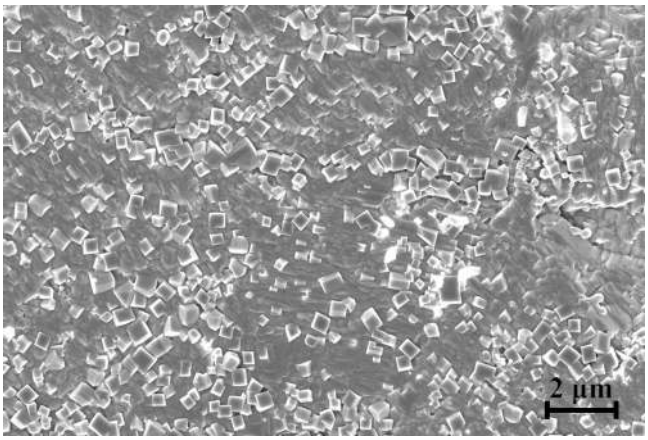

FIG. 1. SEM images of KNN-5%LN ceramics.

grains with an average grain size of 0.6 μm. Figure 2 shows the temperature dependent 10 kHz dielectric constant ε_r and loss factor tan δ for KNN-5%LN taken on heating over the temperature range of 300 to 780 K. Two dielectric peaks can be seen. A sharp dielectric maximum was found near 723 K, corresponding to the Curie temperature T_C. A second broader dielectric peak was observed near 350 K, which has previously been considered to be a O→T transformation.[2,37,43] Compared to pure KNN ($T_C \sim 688$ K and $T_{O\text{-}T} \sim 483$ K),[17,36] the value of T_C was slightly increased; whereas that of $T_{O\text{-}T}$ was decreased by addition of 5% LN. The values of ε_r and tan δ at 300 K were enhanced from 450 and 0.019 for pure KNN (Ref. 36) to 500 and 0.045 for KNN-5%LN. These trends in property changes are consistent with previously reported results for KNN-x%LN.[39,40,42]

Figures 3(a) and 3(b) then show the temperature dependence of the pseudocubic $(200)_{pc}$ and $(222)_{pc}$ diffraction peaks taken on heating at 10 K steps between 280 and 420 K. The $(200)_{pc}$ peak (Fig. 3(a)) shows a triplet splitting below 340 K, and a doublet one above 340 K. Correspondingly, the $(222)_{pc}$ peak (Fig. 3(b)) shows a doublet splitting below 340 K, and no splitting above 340 K. However, at 340 K, both the $(200)_{pc}$ and $(222)_{pc}$ peaks exhibited a mixture of characteristic having four and three peaks, respectively.

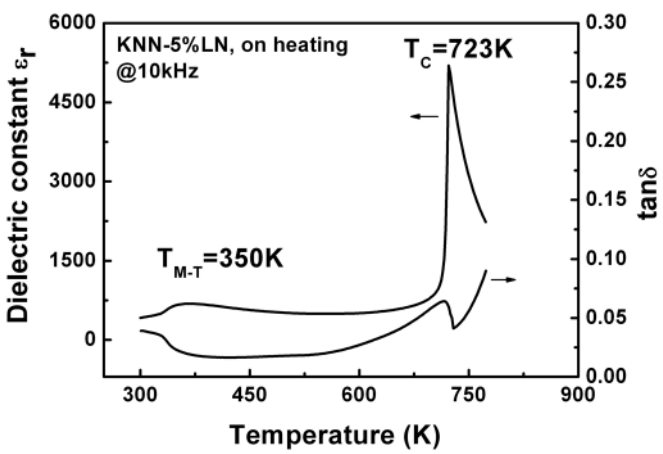

FIG. 2. Dielectric constant ε_r and loss factor tan δ as functions of temperature taken on heating at 10 kHz for $(K_{0.5}Na_{0.5})NbO_3$-5%$LiNbO_3$.

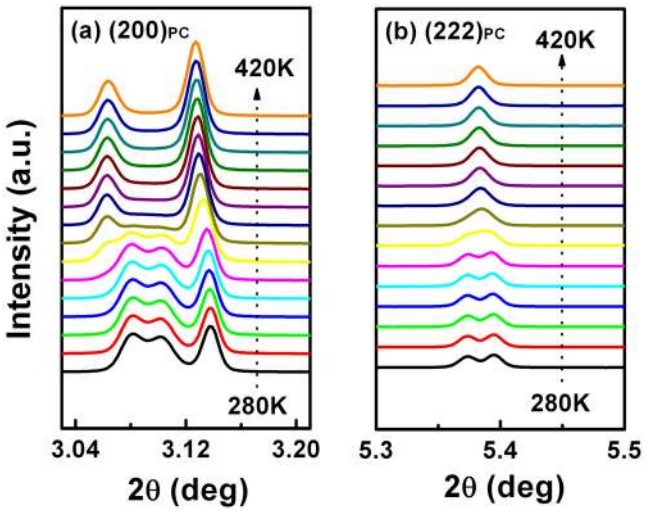

FIG. 3. (a) and (b) Temperature dependence of pseudocubic (200) and (222) diffractions zones taken on heating at 10 K steps from 280 to 420 K for $(K_{0.5}Na_{0.5})NbO_3$-5%$LiNbO_3$.

These XRD results demonstrate that a structural phase transformation occurred near 340 K, as also revealed by the dielectric data (Fig. 2). It is well known that both O and T symmetries should result in a doublet splitting of the $(200)_{pc}$ zone. However, the triplet splitting of the $(200)_{pc}$ zone below 340 K (Fig. 3(a)) demonstrates that the crystal symmetry for KNN-5%LN below 340 K is not orthorhombic.

Figures 4(a)–4(c) show the Rietveld refinement structural analysis at 420 K, 340 K, and 280 K, respectively. Observed and calculated diffraction profiles are shown by cross markers and solid lines. The difference plots are shown below the data in each figure, and the short vertical markers represent the peak positions. At 420 K, the refinement best fit the *P4mm* space group similar to previous reports for $KNbO_3$:[17,60] which produced a good fit with a profile R value of $R_p = 2.20\%$ (see Fig. 4(a) and Table I). At 280 K, the refinement best fit the *Pm* space group, similar to previously reports for $Pb(Mg_{1/3}Nb_{2/3})O_3$-35%$PbTiO_3$:[50,55] with $R_p = 6.05\%$ (see Fig. 4(c) and Table I). However, in the phase transformation region at 340 K, the refinement best fit to a combination of *P4mm* and *Pm* space groups: with R_p=3.05% (see Fig. 4(b)) for volume fractions of 35.7% and 64.3% for T (*P4mm*) and M (*Pm*) phases, respectively. The refined lattice parameters, atomic positions and R_p values of the fitting for the *P4mm* (420 K) and *Pm* (280 K) space groups are given in Table I.

Coexistence of T and O phases for $5 \leq x \leq 7$ has previously been reported for KNN-x%LN:[2,37,41] *P4mm* and *Amm2* space groups were considered for refinements in the temperature range of 280 to 340 K, and dismissed as possible structural models. The observed intensity profiles cannot fully describe a model of *P4mm* and *Amm2* phase coexistence, which gave notably inferior profile R values ($R_p = 26.15\%$ and 8.80% at 280 K and 340 K) than for single phase *Pm* ($R_p = 6.05\%$ at 280 K) or *P4mm* + *Pm* phases ($R_p = 3.05\%$ at 340 K). A comparison of the insets in Fig. 4 highlights the major differences in the $(200)_{pc}$ peaks for both the T and M phases. Due to the relatively low x-ray energies and

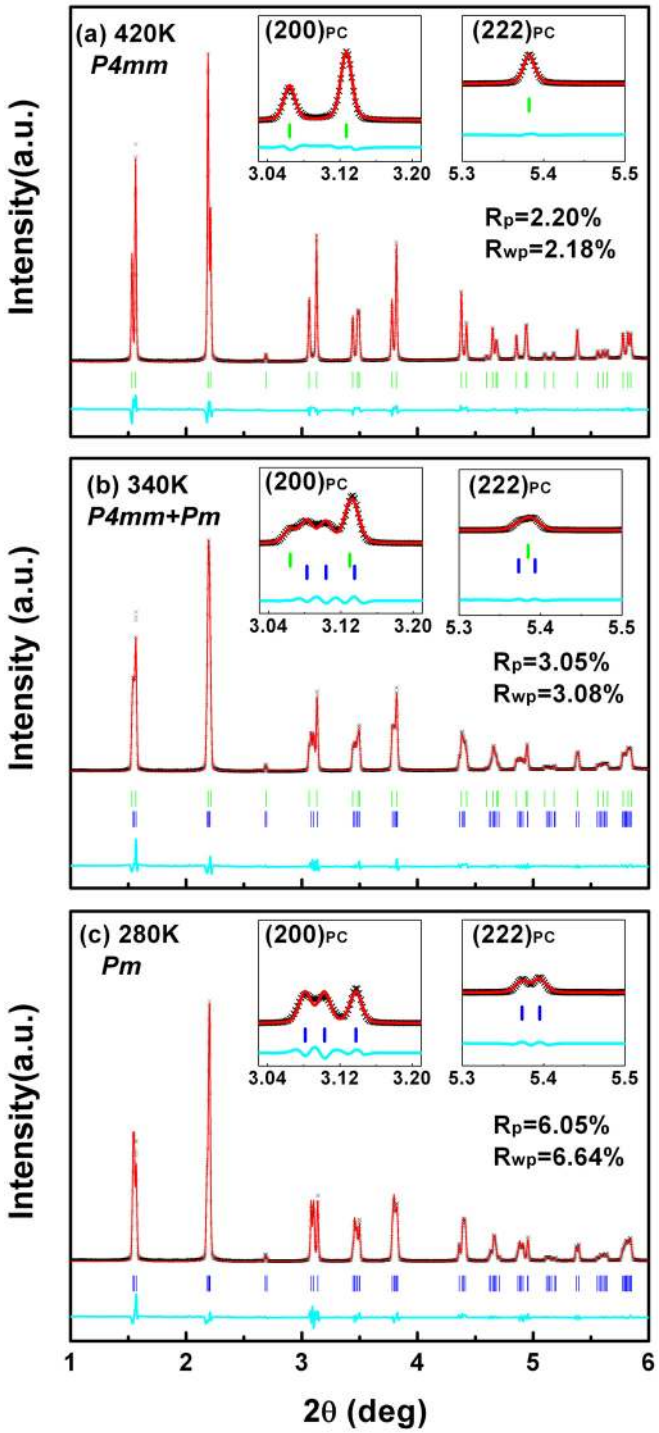

FIG. 4. Observed and calculated (Rietveld refinements) diffraction profiles of (a) the tetragonal phase, (b) tetragonal and monoclinic two phase field, and (c) monoclinic phase for $(K_{0.5}Na_{0.5})NbO_3$-5%$LiNbO_3$: which were taken at temperatures of 420 K, 340 K, and 280 K, respectively. Difference plots are shown, where short vertical markers represent peak positions. The insets in each figure highlight the differences between the tetragonal and monoclinic phases for the pseudocubic $(200)_{pc}$ and $(222)_{pc}$ zones.

subsequent poor resolution of conventional x-ray diffraction systems, previous structural studies[2] have not been able to detect the peak splitting at the low angle side of the $(200)_{pc}$ peaks: as can be seen in insets of Fig. 3(c). This may have contributed to an incomplete interpretation of the structural data for KNN-x%LN for $5 \leq x \leq 7$ in the past.

TABLE I. Structural results for the *P4mm* and *Pm* phases of $(K_{0.5}Na_{0.5})NbO_3$ −5%$LiNbO_3$.

	P4mm (420 K)	*Pm* (280 K)
a, *b*, *c* (Å)	3.95644(5), 3.95644(5), 4.03758(5)	4.0149(1), 3.9431(1), 3.9873(1)
α, β, γ (deg)	90, 90, 90	90, 90.349(2), 90
K/Na/Li	1b (Wyckoff)	1a (Wyckoff)
x, *y*, *z*	0.5, 0.5, 0.2322	0.7124, 0, 0.8500
Nb	1a (Wyckoff)	1b (Wyckoff)
x, *y*, *z*	0, 0, 0.7546	0.2298, 0.5, 0.3339
O1	1a (Wyckoff)	1a (Wyckoff)
x, *y*, *z*	0, 0, 0.2856	0.2582, 0, 0.2903
O2	2c (Wyckoff)	1b (Wyckoff)
x, *y*, *z*	0.5, 0, 0.7124	0.6889, 0.5, 0.3753
O3	…	1b (Wyckoff)
x, *y*, *z*	…	0.1749, 0.5, 0.8542
R_p	2.20%	6.05%
R_{wp}	2.18%	6.64%
χ^2	25.3	39.2
GOF	5.1	6.3
No. of parameters	29	38

Finally, Figure 5 shows the refined lattice parameters for KNN-5%LN as a function of temperature from 280 to 420 K. The temperature evolution of the deviation of the monoclinic angle β from 90° is plotted in the inset of Fig. 5. Between 340 and 360 K, the best refinement was for a model of coexisting $Pm + P4mm$ phases. Below 340 K, the best fit structure was single phase *Pm*: with lattice parameters of (a_m, b_m, c_m; β) = (4.015 Å, 3.944 Å, 3.987 Å; 90.34°) at room temperature. With increasing temperature, it can be seen that monoclinic lattice parameters of a_m and c_m were slightly decreased, whereas b_m was slightly increased with increasing temperature. Between 340 and 360 K, the M phase transformed to a T phase, with lattice parameters of (a_t, c_t) = (3.955, 4.040) Å at 360 K. The temperature evolution of the lattice parameters was continuous in the M and T phases. At the transition temperatures, an abrupt change occurred, and a mixing of the M and T phases was observed. This discontinuity of the lattice

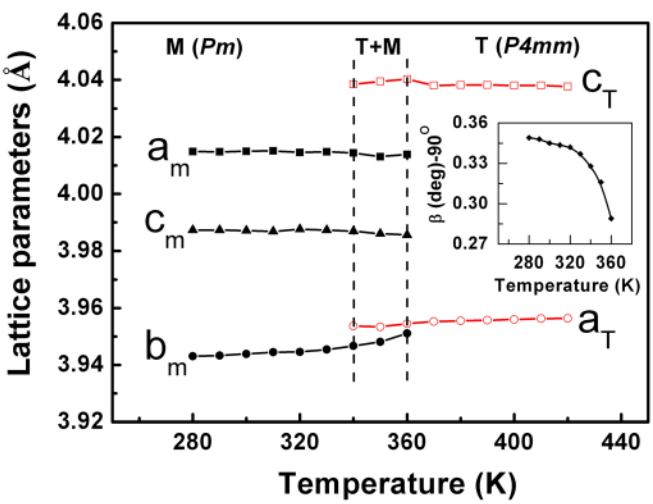

FIG. 5. Lattice parameters of $(K_{0.5}Na_{0.5})NbO_3$-5%$LiNbO_3$ as a function of temperature.

parameters and two phases coexistence at the phase transitions indicate that the M→T phase transition in KNN-5%LN is a first-order phase transition.[34,61,62] The temperature range for coexistence of T and M phases in KNN-5%LN was 120 K lower than that reported for $K_{0.3}Na_{0.7}NbO_3$ (Ref. 21) and $K_{0.56}Na_{0.44}NbO_3$ (Ref. 24) in which the difference between M and O structure was quite small. These results indicate that 5 at. %-Li doping enhanced the monoclinic distortion in KNN.

The M phase observed here for KNN-5%LN has the same space group symmetry *Pm* as previously reported for the "giant" piezoelectric materials of $Pb(Mg_{1/3}Nb_{2/3})O_3$-x%$PbTiO_3$ (Ref. 50) and $Pb(Zn_{1/3}Nb_{2/3})O_3$-x%$PbTiO_3$ (Ref. 54) near their MPBs: previously denoted as the Mc phase.[56] The Mc phase allows the polarization vector to be unconstrained within the psuedocubic (010) plane, rather than constricted to a particular crystallographic axis as for the T or O phases. This means that the polarization vector can be easily rotated within the psuedocubic (010) plane by external electric field, giving rise to an enhanced piezoelectric response due to polarization rotation.[52] Our findings show that a similar Mc phase in KNN-x%LN results in enhanced piezoelectric properties for $5 \leq x \leq 7$.[2] These findings offer new insights in understanding the enhanced piezoelectricity in Pb-free systems containing polymorphic phase boundaries.

IV. CONCLUSION

In summary, we report a monoclinic M_C phase belonging to the *Pm* space group with room temperature lattice parameters of (a_m, b_m, c_m; β)=(4.015 Å, 3.944 Å, 3.987 Å; 90.34°) for KNN-5%LN ceramics. Temperature dependent synchrotron x-ray powder diffraction measurements revealed that the M_C phase transformed to a tetragonal one with space group symmetry of *P4mm* on heating between 340 K and 360 K. These findings demonstrate the presence of structurally bridging low symmetry monoclinic phase in KNN-*x*%LN lead-free solid solution system: indicating a means to achieve high piezoelectricity in lead-free systems via domain engineering.

ACKNOWLEDGMENTS

This work was supported by the Department of Energy under Grant No. DE-FG02-07ER46480, by the National Science Foundation (Materials world network) under Grant No. DMR-0806592, and by the Specialized Research Fund for the Doctoral Program of Higher Education under Grant No. 20090131110015. Use of the APS was supported by the U. S. Department of Energy Office of Science, under Contract No. DE-AC02-06CH11357. The authors also thank Mr. Zhiguang Wang for scanning electronic microscope measurements.

[1]Y. Saito, H. Takao, T. Tani, T. Nonoyama, K. Takatori, T. Homma, T. Nagaya, and M. Nakamura, Nature **432**, 84 (2004).
[2]Y. P. Guo, K. Kakimoto, and H. Ohsato, Appl. Phys. Lett. **85**, 4121 (2004).
[3]E. Hollenstein, M. Davis, D. Damjanovic, and N. Setter, Appl. Phys. Lett. **87**, 182905 (2005).
[4]S. J. Zhang, R. Xia, T. R. Shrout, G. Z. Zang, and J. F. Wang, J. Appl. Phys. **100**, 104108 (2006).
[5]Y. F. Chang, S. F. Poterala, Z. P. Yang, S. Trolier-McKinstry, and G. L. Messing, Appl. Phys. Lett. **95**, 232905 (2009).
[6]J. L. Zhang, X. J. Zong, L. Wu, Y. Gao, P. Zheng, and S. F. Shao, Appl. Phys. Lett. **95**, 022909 (2009).
[7]R. Z. Zuo, J. Fu, and D. Y. Lv, J. Am. Ceram. Soc. **92**, 283 (2009).
[8]D. Tanaka, T. Tsukada, M. Furukawa, S. Wada, and Y. Kuroiwa, Jpn. J. Appl. Phys. (Part 1) **48**, 09KD08 (2009).
[9]Y. Gao, J. Zhang, Y. Qing, Y. Tan, Z. Zhang, and X. Hao, J. Am. Ceram. Soc. **94**, 2968 (2011).
[10]Z. Li, Y. Li, and J. Zhai, Curr.Appl. Phys. **11**, S2–S13 (2011).
[11]S. O. Leontsev and R. E. Eitel, Sci. Technol. Adv. Mater. **11**, 044302 (2010).
[12]W. Liang, W. Wu, D. Xiao, J. Zhu, J. Zhu, and J. Wu, Phys. Status Solidi (RRL) **5**, 220 (2011).
[13]Y. F. Chang, S. F. Poterala, Z. P. Yang, and G. L. Messing, J. Am. Ceram. Soc. **94**, 2494 (2011).
[14]D. Berlincourt, *Ultrasonic Transducer Materials: Piezoelectric Crystals and Ceramics* (Springer, Plenum, London, 1971).
[15]G. H. Haertling, J. Am. Ceram. Soc. **82**, 797 (1999).
[16]B. Jaffe, W. R. Cook, and H. Jaffe, *Piezoelectric Ceramics* (Academic, London and NY, 1971).
[17]G. Shirane, R. Newnham, and R. Pepinsky, Phys. Rev. **96**, 581 (1954).
[18]V. J. Tennery and K. W. Hang, J. Appl. Phys. **39**, 4749 (1968).
[19]M. Ahtee and A. M. Glazer, Acta Crystallogr. **32**, 434 (1976).
[20]M. P. Lemeshko, E. S. Nazarenko, A. A. Gonchar, L. A. Reznichenko, O. Mathon, Y. Joly, and R. V. Vedrinskii, EPL **77**, 26003 (2007).
[21]D. W. Baker, P. A. Thomas, N. Zhang, and A. M. Glazer, Acta Crystallogr. **65**, 22 (2009).
[22]N. Zhang, A. M. Glazer, D. Baker, and P. A. Thomas, Acta Crystallogr. **65**, 291 (2009).
[23]D. W. Baker, P. A. Thomas, N. Zhang, and A. M. Glazer, Appl. Phys. Lett. **95**, 091903 (2009).
[24]J. Tellier, B. Malic, B. Dkhil, D. Jenko, J. Cilensek, and M. Kosec, Solid State Sci. **11**, 320 (2009).
[25]H. D. Megaw, Ferroelectrics **7**, 87 (1974).
[26]A. M. Glazer and H. D. Megaw, Acta Crystallogr. **29**, 489 (1973).
[27]R. E. Jaeger and L. Egerton, J. Am. Ceram. Soc. **45**, 209 (1962).
[28]D. Nuzhnyy, I. Gregora, S. Kamba, and M. Berta, IEEE Trans. Ultrason. Ferroelectr. Freq. Control **56**, 1843 (2009).
[29]J. G. Fisher, D. Rout, K.-S. Moon, and S. -J. L. Kang, J. Alloys Compd. **479**, 467 (2009).
[30]J. G. Fisher, D. Rout, K.-S. Moon, and S. -J. L. Kang, Mater. Chem. Phys. **120**, 263 (2010).
[31]N. Ishizawa, J. Wang, T. Sakakura, Y. Inagaki, and K.-i. Kakimoto, J. Solid State Chem. **183**, 2731 (2010).
[32]Z. Yi, Y. Liu, M. A. Carpenter, J. Schiemer, and R. L. Withers, Dalton Trans. **40**, 5066 (2011).
[33]F. Rubio-Marcos, J. J. Romero, M. S. Martín-Gonzalez, and J. F. Fernández, J. Eur. Ceram. Soc. **30**, 2763 (2010).
[34]A. Kodre, J. Tellier, I. Arčon, B. Malič, and M. Kosec, J. Appl. Phys. **105**, 113528 (2009).
[35]N. Klein, E. Hollenstein, D. Damjanovic, H. J. Trodahl, N. Setter, and M. Kuball, J. Appl. Phys. **102**, 014112 (2007).
[36]L. Wu, J. L. Zhang, C. L. Wang, and J. C. Li, J. Appl. Phys. **103**, 084116 (2008).
[37]K. Wang and J. F. Li, Appl. Phys. Lett. **91**, 262902 (2007).
[38]A. Glazer, Acta Crystallogr. **28**, 3384 (1972).
[39]L. Jianhua, J. Mater. Sci. **46**, 6364 (2011).
[40]S. Wongsaenmai, S. Ananta, and R. Yimnirun, Ceram. Int. **38**, 147 (2012).
[41]K. Wang and J. F. Li, Adv. Funct. Mater. **20**, 1924 (2010).
[42]Z.-Y. Shen, Y.-M. Li, L. Jiang, R.-R. Li, Z.-M. Wang, Y. Hong, and R.-H. Liao, J. Mater. Sci.: Mater. Electron. **22**, 1071 (2010).
[43]X. K. Niu, J. L. Zhang, L. Wu, P. Zheng, M. L. Zhao, and C. L. Wang, Solid State Commun. **146**, 395 (2008).
[44]H. L. Du, W. C. Zhou, F. Luo, D. M. Zhu, S. B. Qu, and Z. B. Pei, Appl. Phys. Lett. **91**, 202907 (2007).
[45]J. S. Kim, C. W. Ahn, S. Y. Lee, A. Ullah, and I. W. Kim, Curr. Appl. Phys. **11**, S149 (2011) .
[46]Y. J. Dai, X. W. Zhang, and G. Y. Zhou, Appl. Phys. Lett. **90**, 262903 (2007).
[47]W. Ge, J. Li, D. Viehland, Y. Chang, and G. L. Messing, Phys. Rev. B **83**, 224110 (2011).

[48]B. Noheda, D. E. Cox, G. Shirane, J. A. Gonzalo, L. E. Cross, and S. E. Park, Appl. Phys. Lett. **74**, 2059 (1999).
[49]B. Noheda, D. E. Cox, G. Shirane, R. Guo, B. Jones, and L. E. Cross, Phys. Rev. B **63**, 014103 (2001).
[50]B. Noheda, D. E. Cox, G. Shirane, J. Gao, and Z. G. Ye, Phys. Rev. B **66**, 054104 (2002).
[51]H. Cao, J. F. Li, D. Viehland, and G. Y. Xu, Phys. Rev. B **73**, 184110 (2006).
[52]H. X. Fu and R. E. Cohen, Nature **403**, 281 (2000).
[53]L. Bellaiche, A. Garcia, and D. Vanderbilt, Physical Rev. Lett. **84**, 5427 (2000).
[54]B. Noheda, D. E. Cox, G. Shirane, S. E. Park, L. E. Cross, and Z. Zhong, Phys. Rev. Lett. **86**, 3891 (2001).
[55]J.-M. Kiat, Y. Uesu, B. Dkhil, M. Matsuda, C. Malibert, and G. Calvarin, Phys. Rev. B **65**, 064106 (2002).
[56]D. Vanderbilt and M. Cohen, Phys. Rev. B **63**, 094108 (2001).
[57]A. P. Hammersley, S. O. Svensson, M. Hanfland, A. N. Fitch, and D. Hausermann, High Press. Res.: Int. J. **14**, 235 (1996).
[58]A. C. Larson and R. B. Von Dreele, Report No. LAUR 86, 2004.
[59]L. W. Finger, D. E. Cox, and A. P. Jephcoat, J. Appl. Crystallogr. **27**, 892 (1994).
[60]A. W. Hewat, J. Phys. C **6**, 1074 (1973).
[61]H. E. Mgbemere, M. Hinterstein, and G. A. Schneider, J. Appl. Crystallogr. **44**, 1080 (2011).
[62]B. Noheda, L. Wu, and Y. Zhu, Phys. Rev.B **66**, 060103 (2002).